Fuel 366 (2024) 131422

Contents lists available at ScienceDirect

Fuel

journal homepage: www.elsevier.com/locate/fuel

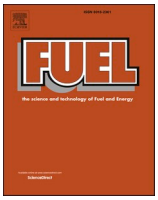

Full Length Article

Soot particles formed by *n*-heptane and *n*-heptane/oxymethylene ether-3 in an inverse diffusion flame: A comparative analysis of chemical features

Ye Liu [a,b], Ran Zhang [c], Jun Wang [c], Yajun Wang [c], Gang Lv [a,*], He Yang [c,*], Haibo Chen [b], Tiezhu Li [d], Bin Hao [e], Junhua Guo [f]

[a] State Key Laboratory of Engines, Tianjin University, Tianjin 300072, China
[b] Institute for Transport Studies, University of Leeds, Leeds LS2 9JT, UK
[c] SINOPEC Research Institute of Petroleum Processing Co., LTD., Beijing, 100083, China
[d] School of Transportation, Southeast University, Nanjing, 210096, China
[e] Yutong Bus Co., Ltd, Zhengzhou, 450016, China
[f] School of Transportation Engineering, East China Jiaotong University, Nanchang, Jiangxi Province, China

ARTICLE INFO

Keywords:
E-fuel
Diesel surrogates
Soot particles
Chemical properties
Diffusion flame

ABSTRACT

Oxymethylene ether-3 (OME_3) is a promising synthetic e-fuel and alternative fuel for diesel engines. In contrast to diesel fuel, the use of OME_3 leads to a distinct combustion process in which soot particles are generated, which leads to changes in the chemical properties of these particles. These chemical properties are intricately connected to both the concentration and availability of potential radical sites, which, in turn, exert a substantial influence on soot oxidation during diesel particulate filter (DPF) regeneration. Hence, it is crucial to investigate the chemical features of soot samples. Nevertheless, a thorough investigation into the chemical features of *n*-heptane/OME_3 soot samples has not been fully understood. Here, X-ray photoelectron spectroscopy (XPS), Fourier transform infrared spectroscopy (FT-IR), elemental analyser, and thermogravimetric analysis (TGA) were used to examine the impact of blending OME_3 on chemical features of soot particles at various flame heights of an inverse *n*-heptane-OME_3 flame. XPS results from C1s and O1s peaks showed that OME_3 incorporation enhanced the concentrations of C = O, C–O, and O = C–O groups, especially C = O groups, with the percentage increase ranging from 11.93 % to 49.74 %. Similarly, the content of aliphatic C – H groups, along with O and H, increased with higher levels of OME_3 blending. Moreover, it was discovered that blending OME_3 altered the spatial distribution of hybridisation orbitals of carbon atoms, leading to a decrease in the sp^2/sp^3 ratio by as much as 40 % with the increase in the OME_3 blending ratio. The alteration in these chemical properties due to the addition of OME_3 enhanced the oxidative reactivity of soot particles, as manifested by up to a 15 % reduction in the measured activation energy. These findings are useful to optimise control strategies of DPF regeneration with the more widespread use of e-fuel.

1. Introduction

Soot particles, which result from the insufficient combustion of various hydrocarbons including oxygenated forms, pose a primary environmental challenge, particularly in urban environments [1–3]. In light of the cancer-causing potential of soot particles for human health, alongside their negative effects on global climate change, the regulations governing soot particles from combustion appliances have been tightened significantly [4–6]. To lessen soot emissions from combustion appliances as well as the carbon footprint, the use of oxygenated alternative synthetic fuels is recognised as a feasible route. Among the numerous oxygenated alternative fuels available, oxymethylene ethers (OME_n), $CH_3O(CH_2O)_nCH_3$, have received more attention due to the following advantages: (1) OME_n are classified as e-fuels, are non-toxic, and can be generated by reprocessing CO_2 through electrolysis powered by renewable energy [7,8]. (2) They are readily miscible with diesel fuel and are utilised directly without significant alterations to the diesel engines [9]. (3) The molecular structure of OME_n lacks C – C bonds, thereby effectively suppressing the formation of key precursors to soot formation, such as C3 and larger hydrocarbon creatures [10]. (4)

* Corresponding authors.
E-mail addresses: lvg@tju.edu.cn (G. Lv), yanghe.ripp@sinopec.com (H. Yang).

https://doi.org/10.1016/j.fuel.2024.131422
Received 3 October 2023; Received in revised form 9 January 2024; Accepted 5 March 2024
Available online 11 March 2024

OME_n, with an oxygen content of 42 % to 50 %, are widely believed to be effective at lowering soot levels [11,12]. (5) OME_n have also demonstrated positive effects in reducing carbon monoxide (CO) and unburned hydrocarbons when OME_n is applied as an additive to diesel engines [13–15].

Among the OME_n, OME_3 is the most compact compound suitable for real-world uses, which possesses an appropriate cetane number (78), melting point (-41 C), and boiling point (156 C) [8,10]. Compared to OME_3, OME_1 possesses a low cetane number of 29 and a correspondingly low boiling point of 42 °C. Consequently, the high volatility renders it susceptible to vaporization in storage [10]; OME_2 possesses an acceptable cetane number of 63, but its flash point exceeds the minimum required to satisfy safety standards [16]; By contrast, OME_4 is more difficult to use, with its cetane number (90), melting point (-7 C) and boiling point (202℃) [9]. OME_n with $n > 5$ possesses an excessively high melting point. Moreover, OME_3 demonstrates superior low-temperature fluidity and volatility than OME_4 and OME_5, enhancing fuel vapour evaporation and thus improving spray performance. Therefore, OME_3 emerged as an ideal contender for use as a fuel additive and was the subject of the current research. Nevertheless, several potential challenges are associated with the real-world application of OME_3. Among them, economic factors are particularly significant. For example, the total monetized cost of OME_3 is estimated to be 1.5 to 3.6 times that of traditional fossil-based diesel [17].

The influence of blending OME_n on soot emissions has been well documented in previous research. For example, Pellegrini et al. [18,19] explored the influence of incorporating OME on PM emissions generated from a light-duty diesel engine and found that incorporating 10–12 % OME into diesel could cause a 40 % decrease in PM emissions. García-Oliver et al. [12] studied the effects of various stoichiometries of OME on the in-cylinder combustion behaviour and pollutant formation when blended with fossil diesel using numerical simulations and experimental testing. The results showed that increasing the OME content in the blend above 30 % led to faster combustion and significantly reduced soot formation. Schmitz et al. [20] investigated the soot particle formation and chemical features in laminar premixed flames fueled with ethylene/$OME_{2\text{-}4}$ flames. They observed that $OME_{2\text{-}4}$ blended flames exhibited a reduction in the total number and size of soot particles, along with a higher presence of oxygenated functionalities compared to pure ethylene flames. Furthermore, Schmitz et al. [21] found that OME_n had a significant impact on reducing the formation of larger soot particles in premixed flames, while the formation of smaller particles remained relatively unchanged. Gelner et al. [22] examined the particle emissions of a heavy-duty engine fueled with OME. The results showed that the majority of the nuclei mode particles generated from the OME operation were volatile in nature and solid particle number emissions were below compared to Euro VI diesel operation. Ma et al. [23] reported blending OME_3 with diesel fuel can significantly reduce particulate matter emissions from a diesel engine, including black carbon and organic carbon. Arias et al. [24] studied the exhaust emissions with the use of OME as a diesel fuel substitute in a Euro 6 engine under the Worldwide harmonized Light vehicle Test Cycle. They reported that the 20 % OME blends resulted in a 61 % reduction in particle number emissions and a 41 % increase in NO_x emissions compared to diesel fuel. Tan et al. [9] observed an interesting phenomenon regarding the impact of blending OME_3 on flame-formed soot emissions. Upon blending OME_3 with ethylene at a 5 % concentration, an approximate 10 % rise was observed in the soot volume fraction. They attributed the increase in PM to the fact that small amounts of OME_3 can promote the production of large numbers of C2 species, which favour the formation of soot particles. However, upon increasing the proportion of OME_3 to higher than 10 %, the volume fraction of soot particles diminished in comparison to that of the pure ethylene flame. Moreover, comparative research was carried out to assess the suppressive effect of OME_n ($n = 1$–4) and other oxygenated fuels on the tendency of diesel diffusion flames to produce soot [25]. The results showed that the most substantial impact on soot reduction was achieved by diluting the aromatic content of diesel fuel, followed by reducing the chain length of hydrocarbons and raising the amount of oxygen in the fuel. Ferraro et al. [8] examined the influence of introducing OME_3 on soot particles and observed a decrease in both the overall quantity and the dimensions of soot particles across all equivalence ratios following the inclusion of OME_3. To summarise, these studies primarily addressed the potential roles of OME blending in the reduction of soot particles. However, few studies focused on how OME blending affects the chemical properties of soot particles.

The chemical properties of soot particles would significantly affect the rate of oxidative regeneration of soot particles deposited on diesel particulate filters (DPFs) [26–28]. For instance, the presence of aliphatic C–H groups of soot particles significantly decreased as soot particles became inactive and underwent graphitisation, meaning that greater concentrations of aliphatic C–H groups were associated with increased reactivity in soot oxidation [29,30]. Guo et al. [31] revealed that soot samples generated from oxygenated fuels have a higher concentration of oxygenated functional groups on the edge plane, which in turn are more susceptible to oxygen attacks. Wei et al. [27,32] explored the potential factors affecting soot reactivity through Partial Least Square analysis, revealing that chemical properties of soot particles (i.e., surface functional groups and hybridised carbon atoms), were crucial factors governing soot reactivity. Guo et al. [31] found that soot samples from oxygenated fuel blends were generally more reactive and had more oxygen functional groups on the carbon layer edge plane. Sun et al. [33] discovered that soot particles with greater amounts of oxygen and surface oxygen-containing groups had higher oxidative reactivity. Furthermore, their results also revealed a significant correlation between the content of defective graphitic carbon and the oxidative rate of soot particles. Lapuerta et al. [34] summarised that the presence of aliphatic and oxygenated functional groups of soot particles was intricately linked to oxidative reactivity, which was crucial for both active and passive regeneration processes of DPFs. At the same time, the incorporation of OME_3 as an alternative to diesel fuel inevitably resulted in modifications to the chemical properties of soot samples. To our knowledge, however, a comprehensive investigation into the chemical features of soot particles generated from OME_3-added fuels has not been conducted.

Given these motivations and the identified research gaps, we investigated the impact of blending OME_3 into *n*-heptane on the chemical properties of soot particles at various phases in an inverse diffusion flame. Soot particles were sampled during the formation, growth, and oxidation phases. X-ray photoelectron spectroscopy (XPS), Fourier transform infrared spectroscopy (FT-IR), elemental analyser, and thermogravimetric analysis (TGA) were used to characterise the chemical properties of soot particles, including the O/C ratio, surface functional groups, hybridised orbitals of carbon atoms, elemental composition, and oxidative reactivity. The obtained results are anticipated to establish a theoretical foundation for the implementation of OME_3 in the real world.

2. Experimental

2.1. Burner setup

Fig. S1 of the Supplementary material provides the schematic illustration of the testing system. In this study, the McKenna water-cooled burner was used, featuring a central tube of 12.7 mm (ID) for the oxygen and nitrogen mixture, an intermediate annular bronze porous plug of 30 mm (ID) to deliver the fuel, and an outer bronze porous plug of 75 mm (ID) that serves a shield to avoid the formation of secondary flames with ambient air. The burner setup was affixed to a motorised translation platform with a precision of ± 0.005 mm, enabling vertical adjustments for fine-tuning the sample collection position. The W-102A Bronkhorst vapour delivery system was used to vaporise liquid fuel (n-heptane/OME_3) at 423 K. In the liquid fuel stream, Argon with a purity

of 99.999 % was used to transport the vaporized fuel to the burner via heated tubes kept at 473 K. To avoid the condensation of fuel within the burner, a coil heater was employed to raise the temperature of both the gaseous oxygen and nitrogen mixture and shielding nitrogen, to a level of 423 K. The flow rates of liquid fuel and carrier gas (Ar) were configured with Bronkhorst digital flow controllers, which have a precision of 0.02 % and 0.2 %, respectively. OME_3 was added by substituting a portion of the *n*-heptane (10 % and 20 % of the total carbon, terms OME-10 and OME-20) fed to the reference *n*-heptane flame. While adding OME_3, the velocity of cold gas and the overall flow rate of carbon remain almost constant maintained nearly constant. The specific flow rates of the fuel stream in the current study are listed in Table 1. The same method was applied when examining other alternative fuels [25,35]. The flow rates of oxygen, nitrogen, and shielding nitrogen were meticulously controlled using digital mass flow controllers with a precision of ± 0.2 %. These flow rates were specifically adjusted to 0.52 L/min for oxygen, 0.6 L/min for nitrogen, and 55 L/min for shielding nitrogen at a temperature of 293.15 K.

2.2. Soot sampling

A probe sampling system was used to collect soot particles at different heights above the burner (HAB), specifically at 20, 40, and 60 mm along the central axis of the diffusion flame [36,37]. A stainless-steel probe of the sampling system, featuring a diameter (3.175 mm) and wall thickness (0.125 mm), was placed in a horizontal orientation directly above the burner. In addition, the midpoint of the probe includes a 0.15 mm sampling orifice through laser drilling, directing its aperture downward to facilitate sampling of the combustion gases as they enter, which was linked to a vacuum to gather soot particles via a Teflon filter. Cold nitrogen gas, flowing at 26.8 L/min, was employed to dilute the drawn combustion gases to effectively halt chemical reactions within the sampling line. Additionally, this dilution process ensured that soot particles were collected at a comparatively low temperature. More comprehensive details about the probe sampling technique have been reported in previous studies [36,38,39]. The duration of collection for each experiment differed depending on the sampling location. Typically, more time was needed when sampling was done at lower flame positions compared to higher ones. Following sampling, the soot particles were gently removed from the filter and gathered for analysis, without undergoing any prior treatment. The temperatures of the central axial flame were quantified by means of an R-type thermocouple (Pt/Pt13 Rh), featuring a wire of 75 μm and a 150 μm bead. The temperatures obtained were adjusted for radiative heat loss using the approach reported by Mcenally et al. [40]. The measured temperatures of sampling positions are summarised in Table 2. The observed fluctuation in flame temperature resulting from the introduction of OME_3 was found to be well within the margin of experimental error. Consequently, the influence of OME_3 upon flame temperature can be deemed insignificantly consequential.

2.3. Soot characterization

XPS was used in this study using an Mg Kα X-ray source from the PerkinElmer PHI-1600 ESCA instrument under ultra-high vacuum conditions to ascertain the oxygenated functional groups and hybridised orbitals of carbon atoms of soot particles. The internal standard for binding energy calibration involved utilising the C1s peak of the contaminant carbon, with a binding energy of 284.6 eV. The XPS data obtained from three discrete regions within each soot sample were subjected to averaging, yielding results with an associated uncertainty of less than 6 %.

Table 2
Flame temperatures of sampling positions along the centerline.

HAB (mm)	Flame temperature of sampling positions (K)		
	n-heptane flame	OME-10 flame	OME-20 flame
20	1546 ± 50	1532 ± 65	1540 ± 61
40	1161 ± 50	1163 ± 63	1143 ± 55
60	942 ± 60	923 ± 63	935 ± 62

The quantification of aliphatic and aromatic C − H groups within the soot samples was conducted using an FT-IR (Nicolet Nexus 470). FT-IR spectra spanning the spectral range of 600–3200 cm^{-1} were obtained, employing a resolution of 1 cm^{-1}. The soot samples were homogenized and finely ground with KBr. To maintain uniformity in the mixture of the soot samples and KBr, a consistent weight percentage of 0.5 % was employed for all samples. Following this, an identical mass of the resultant powder mixture was compressed to form a disc of approximately equal thickness to minimize the experimental error utilising a pressure force of 10 tons for 5 min. Before analysis, the spectra were smoothed and adjusted for baseline corrections. The OMNIC software package was employed for the baseline correction by subtracting the background from the sample spectra. To ensure the reproducibility of the experimental results, we conducted three separate spectra measurements for each sample. It was found that the variations in the FT-IR data were below 5 %.

The elemental composition of soot samples was determined using an Elemental Analyser (Elementar vario EL III). Before conducting the analysis, the soot samples, each weighing approximately 2 mg, underwent a thermal treatment in an oven preset to 105 °C for 3 h. This procedure was undertaken to eliminate any moisture contained within the combustion byproducts or that had condensed from the surrounding atmospheric conditions. The treated soot particles, due to their sensitivity to environmental moisture, were wrapped in a moisture-sealing film. To ensure the reliability of our results, we conducted a minimum of three repetitions for each sample.

TGA (Mettler-Toledo TGA/DSC1) was employed to obtain the activation energy (E_a) to assess the oxidative reactivity of soot particles. The E_a was assessed by non-isothermal TGA. The detail on the method for determining the E_a was reported in our previous work [30,39]. Before each experimental procedure, the soot particles were subjected to heating at 500 °C under a nitrogen flow of 60 ml/min for a duration of 60 min to remove volatile compounds. Thereafter, the temperature was decreased to 200 °C. Subsequently, the sample underwent heating at a rate of 5 °C/min up to 800 °C in an atmosphere of ultrahigh purity air flowing at 60 ml/min. To ascertain the experimental uncertainty, this test was conducted three times for each soot sample.

3. Results and discussion

3.1. Oxygenated functional groups

XPS analysis was carried out to elucidate the impact of incorporating OME_3 on surface compositions and oxygenated functional groups of soot

Table 1
Setting parameters for the fuel flow.

Fuel	Flow rate of N_2 (L/min)	Mass flow rate of *n*-heptante (g/min)	Mass flow rate of OME_3 (g/min)	Carbon flow rate (g/min)	Flame height (mm)
n-heptane	0.31	1.17	0	0.98	70
OME-10	0.31	1.05	0.22	0.98	68
OME-20	0.31	0.93	0.44	0.98	65

samples. The identification of oxygen compositions was attained through the analysis of photoelectron kinetic energy. Fig. S2 of the Supplementary material shows a representative XPS scan of *n*-heptane soot at HAB = 20 mm. To facilitate an elemental comparison, we quantified the O/C atomic ratios by analysing the respective areas under the O 1 s and C 1 s peaks. The O/C atomic ratios for soot particles derived from *n*-heptane and OME_3 addition are illustrated in Fig. 1. The O/C ratios of *n*-heptane soot particles varied from 0.13 to 0.05 as the HAB increased. Correspondingly, the O/C ratios after the addition of OME_3 were in the range of 0.08——0.18, in response to changes in OME_3 content and HABs. Comparing *n*-heptane and OME_3 soot particles revealed that the OME_3 addition in amounts of 10 % and 20 % led to an elevation in O/C atomic ratios. This phenomenon may be attributed to the following factors: The introduction of oxygenated fuels is expected to postpone the initial soot particle formation region within the flame, resulting in the production of a greater quantity of nascent soot particles, which are mostly oxidised and possess a lower C content [41–43]. On the other hand, not all oxygen atoms from the oxygenated fuel during the combustion process are fully used to oxidize carbon into carbon dioxide or carbon monoxide. Some oxygen atoms may be entrapped within the complex structure of the soot particles, resulting in an elevation in the O/C ratio in soot particles [44]. Zhang et al. [45] reported similar values of O/C ratios of soot particles derived from diffusion flames of oxygenated and non-oxygenated fuels. However, they pointed out that the O atoms within soot particles may not originate from the oxygen bound within the fuel.

Most of the O atoms identified through XPS analysis are found within oxygenated functional groups that are chemically bonded to the soot surface, which are closely related to the oxidative reactivity of soot particles [46,47]. As a result, it is essential to quantify the oxygenated functional groups. The overlapping C1s peaks in the XPS spectrum were deconvoluted (see Fig. 2a), and the fitted peaks situated at 288.4 and 286.6 eV were respectively allocated to the C = O groups in carbonyl and C–O groups in epoxy and hydroxyl [47,48]. In addition, the O 1 s peak of the XPS spectrum was deconvoluted to provide valuable insights into the development of oxygenated functional groups with the addition of OME_3 [49]. The peak assignments are as follows [50,51], as shown in Fig. 2b: (1) the values between 530 and 532 eV represent C = O groups in substances like carbonyl and/or carboxylic acid; (2) 531–534 eV corresponds to the C–O groups in epoxy, hydroxyl and/or ether; (3) 530–532 eV is indicative of the O = C–O groups in carboxylic acid and/or ester.

The content of oxygenated functional groups, as determined from the C 1 s and O 1 s peaks, are illustrated in Figs. 3 and 4. From Fig. 3, an increase in the blending content of OME_3 resulted in a consistent rise in the concentration of C − O groups in epoxy and hydroxyl as well as C = O groups in carbonyl. The concentration of defective sites on soot surfaces increases with the incorporation of higher proportions of biofuel in the blended fuel [52,53]. Thus, it makes sense that blending a higher proportion of OME_3 into the mixed fuel would increase relative concentrations of C − O groups in epoxy and hydroxyls as well as C = O groups in carbonyls, given the oxygen atoms preferentially bind to the defective sites to form oxygenated functional groups [54]. However, the increased concentrations of oxygenated functional groups could potentially lead to allergic reactions, respiratory as well as cardiovascular problems, and even cancer if breathed in [55]. The increase percentage of C − O carbonyl groups was between 1.78 % and 30.97 %, while the increase percentage of C = O carbonyl groups ranged from 11.93 % to 49.74 % as the OME_3 blending ratio increased. Compared to C − O epoxy and hydroxyl groups, the increased percentage of C = O carbonyl groups was relatively larger. This phenomenon is because the existence of C–O bonds and the lack of C–C bonds within the fuel framework would promote the formation of C = O carbonyl groups [7]. As a result, this leads to a more significant rise in the increased percentage of C = O carbonyl groups. The oxygenated functional groups create more active sites on the soot surface, facilitating the adsorption of oxygen molecules [56]. Thus, an increase in these oxygenated functional groups with the increasing OME_3 would enhance the oxidative reactivity of soot particles.

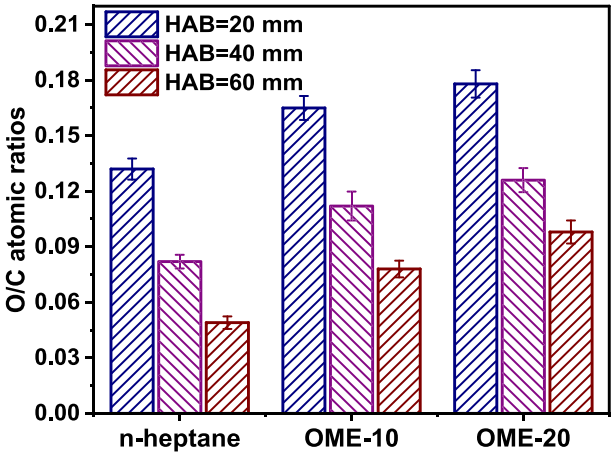

Fig. 1. O/C atomic ratios for soot particles from *n*-heptane and OME_3 addition at various HABs.

From Fig. 3, both oxygenated functional groups decreased for all soot particles as the HAB increased. As the oxidation and gasification reactions proceed further, accompanied by an increase in the HAB, the defective sites bond to oxygenated functional groups may be oxidised, and the intermediate oxygenated groups may be broken down during gasification, leading to a decrease in oxygenated functional groups [54,57]. The reduction percentage of C = O carbonyl groups with increasing HAB ranged from 4.38 to 15.01 %, which was smaller than the decrease in C − O groups in epoxy and hydroxyl (13.97–29.22 %). This observation is unexpected according to the relatively poorer thermodynamic stability of C = O carbonyl groups [48]. The observed results can be explained by the following fact. As found in references [54,58], the formation of C − O groups predominantly occurs in the early stages of oxidation at relatively lower HABs, while more C = O carbonyl groups are formed as oxidation proceeds further at higher HABs, leading to a slower rate of decline of the C = O carbonyl groups.

The results from the O 1 s spectrum, as illustrated in Fig. 4, showed that C − O groups for all soot particles were the most dominant surface species within soot particles. The concentrations of oxygenated functional groups were observed to increase for soot samples at the same HAB with increasing OME_3 doping. The C − O groups were the most prominent among oxygenated functional groups, followed by the C = O and O = C − O groups. It should be noted that the O = C − O groups in ester and acid contribute less to oxidation reactions. This is because ester and acid functionalities tend to undergo decarboxylation rather than participate in oxidation reactions [59]. As the proportion of OME_3 increased, the increased percentage of oxygenated functional groups within soot particles was the largest of C = O groups, ranging from 13.85 % to 26.41 %, followed by O = C − O and C − O groups, in line with the results from the C 1 s spectrum. Moreover, the percentage reduction regarding C − O, C = O, and O = C − O groups ranged from 12.16 % to 15.38 %, from 8.61 % to 12.84 %, and from 5.03 % to 8.21 %, respectively, when the HAB increased. It means that among these oxygenated functional groups, the decreased percentage of O = C–O groups was the smallest with the increase of HAB. As revealed by Fanning and Vannice [60], the initial formation of C–O groups in cyclic ethers would undergo rearrangements to generate bridges resembling ethers, connecting polyaromatic regions and subsequently forming cyclic anhydrides as the oxidation reactions proceeded. Eventually, these cyclic anhydrides would further develop into carboxylic acids including O = C–O groups. Although a large number of O = C–O groups are consumed as oxidation proceeds, some carboxylic acids, including the O = C–O group, are produced. As a result, the decreased percentage of the

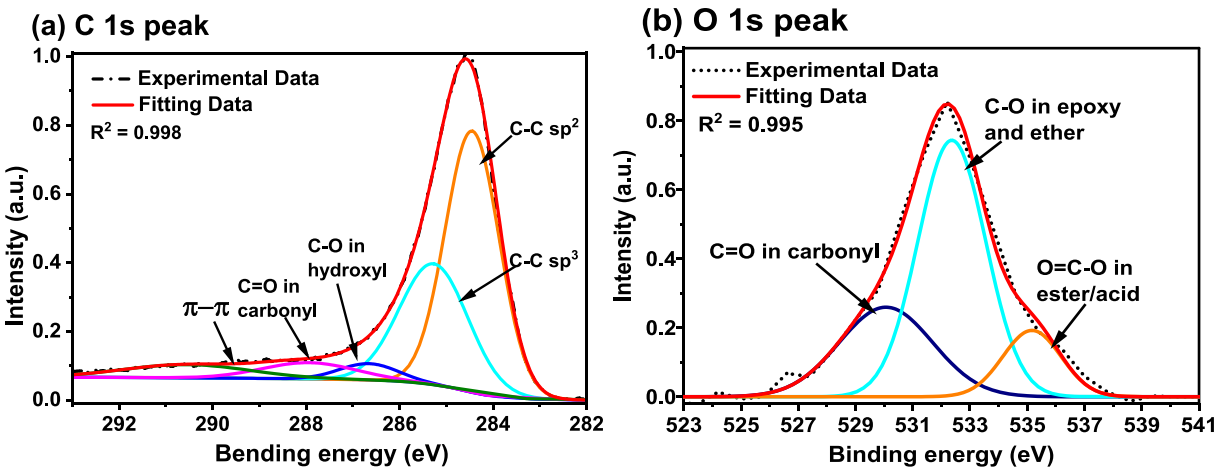

Fig. 2. Representative XPS C 1 s (a) and O 1 s (b) peaks, along with their corresponding fitting peaks of *n*-heptane soot sample at HAB = 20 mm.

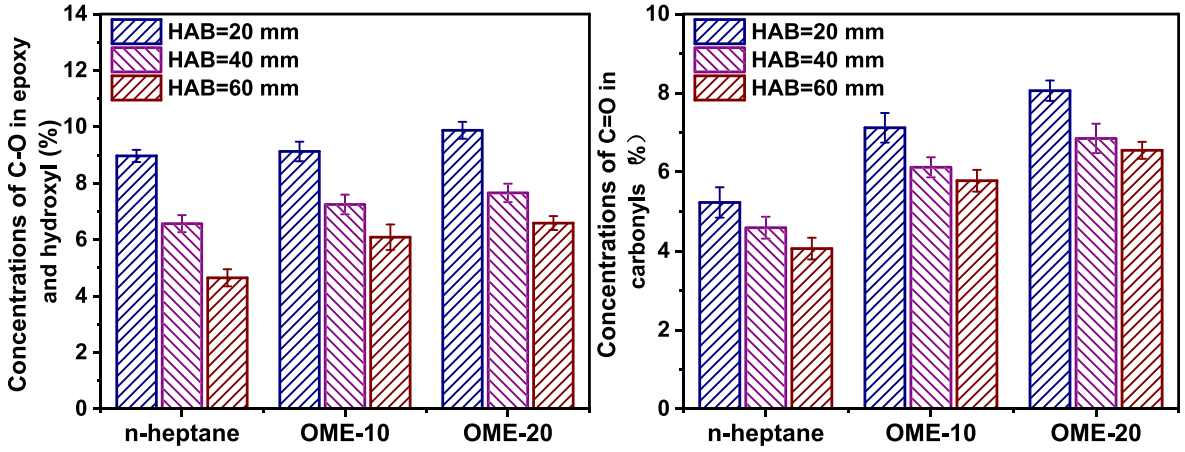

Fig. 3. Relative concentrations of oxygenated functional groups for soot particles from *n*-heptane and OME_3 addition at various HABs.

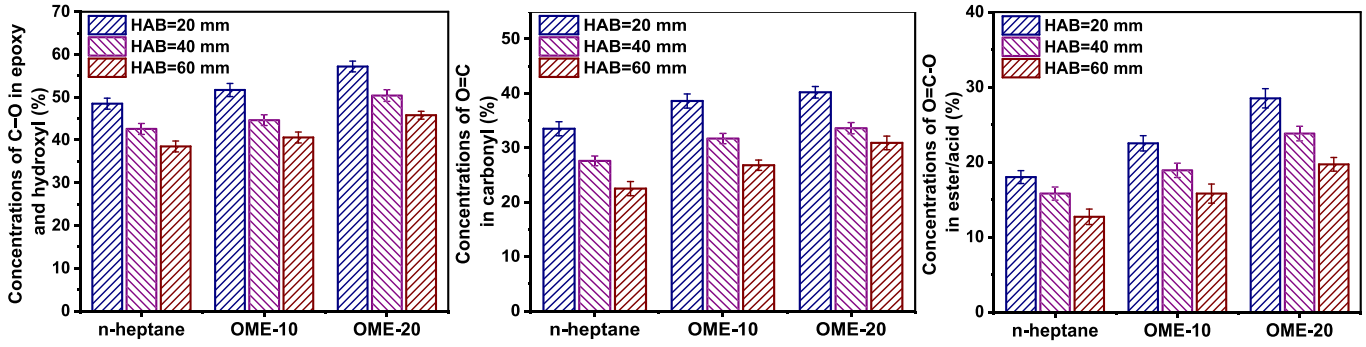

Fig. 4. Relative concentrations of oxygenated functional groups for soot particles from *n*-heptane and OME_3 addition at various HABs.

cumulative amount of O = C–O groups was the smallest as the HAB increased.

3.2. Hybridised orbitals of carbon atoms

The primary hybridized orbital forms of carbon atoms within soot particles are the sp^2 and sp^3 bonding states, and the oxygenated functional groups can interact with these sp^2 and sp^3 bonding states [47]. As a result, to evaluate how the incorporation of OME_3 affects hybridised orbitals of carbon atoms within soot particles, it is required to obtain information regarding the sp^2 and sp^3 bonding states. Similar to the deconvolution procedure applied to the oxygenated functional groups, two deconvoluted peaks segregated from the C 1 s peak are illustrated in Fig. 2a. The peaks, located at around 284.3 eV and 285.4 eV, are associated with sp^2 and sp^3 hybridised C atoms, respectively [42,52]. The sp^3-hybridised C atoms correspond to defective sites capable of breaking the sp^2-hybridised network, requiring bond termination apart from neighbouring π-bonded C atoms [47,62]. These sp^3-hybridised C atoms diminish long-range order and are therefore regarded as defective sites [47,49,63]. This means that a decreased ratio of sp^2/sp^3 hybridisation is indicative of a structure that is more disordered and amorphous.

Fig. 5 illustrates the variation of the sp^2/sp^3 hybridization ratio with

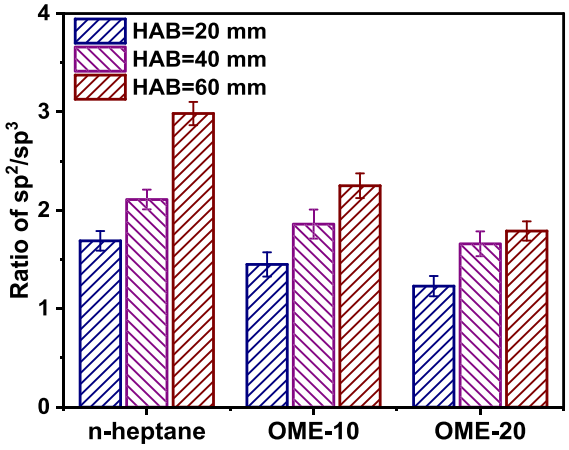

Fig. 5. Sp^2/sp^3 hybridisation ratios for *n*-heptane and OME_3-added soot particles at various HABs.

respect to HABs for *n*-heptane and *n*-heptane/OME_3 soot particles. It can be seen that the sp^2/sp^3 values reduced with an increase in OME_3 content, indicating a decrease in graphitic planar structures or an increase in amorphous structure within the soot. The impact of OME_3 on the gas phase pathways is likely responsible for variations in the carbon bonding states of soot particles [8]. One potential advantage of oxygen in the fuel structure is the facilitation of decomposition and oxidation processes, resulting in a drop in the total quantity of precursors and consequently, a reduction in the aromatic sp^2 network. Furthermore, the oxygen in the fuel structure would promote the creation of small oxygenated polycyclic aromatic hydrocarbons (PAHs) or other oxygen-containing molecules bonded to defective sites, increasing the concentrations of sp^3 hybridised C atmos. Thus, there was a decrease in the ratio of sp^2/sp^3 hybridisation with increasing OME_3. The decreased sp^2/sp^3 ratio indicates higher tortuosity of fringes within soot particles, which makes soot more susceptible to oxygen attack [64], and thus enhances the oxidative reactivity of soot particles.

Moreover, it is observed from Fig. 5 that the ratio of sp^2/sp^3 hybridisation showed an increase with increasing HAB. This phenomenon is likely due to the selective oxidation of various carbon structures. The oxidation reactions continue to proceed with the increase of HAB. The smaller microcrystalline carbon layers with a higher proportion of sp^3 hybridisation states are consumed more easily, leaving those larger microcrystalline carbon layers with a higher proportion of sp^2 hybridisation states [52,65]. Therefore, the ratios of sp^2/sp^3 increased for all the soot samples with the increase of HAB.

3.3. C – H functional groups

FT-IR was utilised to examine the variation in the aliphatic and aromatic C–H functional groups on the soot surface when different blends of *n*-heptane and OME_3 were employed. Fig. S3 of the Supplementary Material illustrates a representative FT-IR spectrum of *n*-heptane soot after baseline correction and smoothing, generated at the HAB of 20 mm. According to the approach reported by Mckinnon et al. [66] and our previous studies [29,38,62], the relative concentrations of aliphatic C – H groups were calculated by dividing the intensity of the aliphatic C – H peak at 2920 cm^{-1} by the aromatic C = C peak at 1600 cm^{-1} (I_{2920}/I_{1600}). This approach can effectively avoid the influence of the KBr tablet's thickness and concentration. Fig. 6 displays the ratio values of I_{2920}/I_{1600} for all soot samples at various HABs. The relative concentrations of aliphatic C – H groups were found to rise on soot surfaces at the same sampling location as the OME_3 content increased. Aliphatic C – H groups predominantly arise from the presence of methyl, methylene, and methine groups bonded to aromatic rings on PAHs or from methylene bridges, often of the fluorene type, that maintain network-

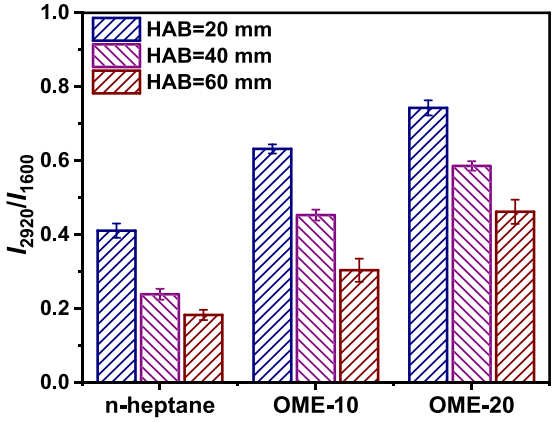

Fig. 6. Relative contents of aliphatic C – H groups for soot samples from *n*-heptane and OME_3 addition at various HABs.

like interconnections between these PAHs [66,67]. Larger amounts of odd-number carbon rings within the planar structure are generated due to the addition of OME_3, thus disrupting the carbon framework and providing more active sites for bonding of aliphatic C – H groups [45,48,64]. Consequently, there was an increase in the I_{2920}/I_{1600} ratios with increasing OME_3 content. H atoms within aliphatic C–H groups require lower energy for abstraction compared to those in aromatic C–H groups [61]. This lower energy requirement leads to the preferential removal of aliphatic hydrogens. As a result, an increase in aliphatic C–H groups indicates more active sites exposed, making them more vulnerable to oxygen attack [68].

As depicted in Fig. 6, it is discernible that the relative concentrations of aliphatic C – H groups for all soot samples exhibited a decline with increasing HAB. It means that as the HAB increased, a large amount of these groups was consumed on soot surfaces. This phenomenon is probably attributable to the ongoing carbonization reactions that occur with the increasing HAB. Similar findings were reported by Dobbins et al. [69,70], who found that aliphatic hydrogen content was reduced due to continuous carbonization reactions with an increase in HAB. Vander Wal et al. [71] also highlighted that the carbonization process of soot particles with increasing flame height led to a reduction in the hydrogen content within soot particles.

In addition to aliphatic C – H groups, the relative content of aromatic C – H groups was determined by calculating the ratio of the intensity of the aromatic C – H peak at 880 cm^{-1} and the aromatic C = C peak at 1600 cm^{-1} (I_{880}/I_{1600}), and the data determined are presented in Fig. 7. Unlike aliphatic groups, soot samples from the *n*-heptane/OME_3 flame

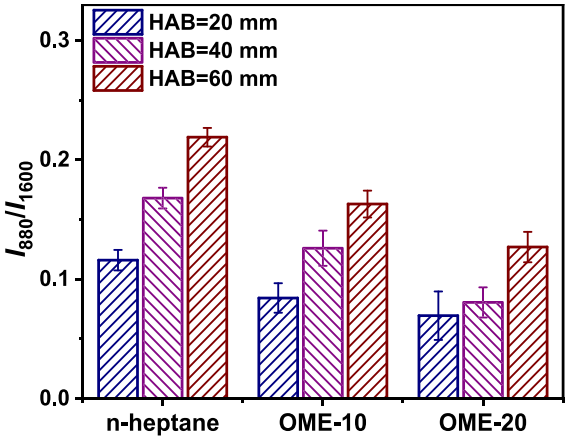

Fig. 7. Relative contents of aromatic C – H groups for soot particles from *n*-heptane and OME_3 addition at various HABs.

exhibited slightly lower contents of aromatic C − H groups in comparison with those from the *n*-heptane flame, indicating that the addition of OME_3 would suppress soot aromatization. Similar findings were reported by Ferraro et al. [8], who demonstrated that soot particles from ethylene/OME_3 flames presented smaller sizes and lower levels of atomization compared to those from pure ethylene flames. Moreover, in contrast to the decreasing trend of aliphatic C − H groups, the relative content of aromatic C − H groups for all soot particles increased with increasing HAB. This phenomenon is probably because the aliphatic structures within soot particles undergo de-alkylation and/or cyclization reactions, ultimately leading to an increase in the relative contents of aromatic structures [72]. Similarly, Santamaria et al. [73,74] revealed a progressive aromatization process in soot particles as the HAB increased, accompanied by a reduction in aliphatic characteristics. The results obtained by Mckinnon et al. [66] demonstrated a progressive rise in the aromatic composition of soot particles with increasing HAB, concomitant with a gradual decline in the aliphatic content.

3.4. Elemental analysis

Table 3 provides information on the weight percentage (wt %) of elemental composition for soot samples, along with the H/C and O/C atomic ratios. It is evident that soot samples predominantly comprise C, H, and O atoms. The C and H contents were determined through elemental analysis, while the O content was calculated by deducting the weight percentages of C and H from 100 %. It is obvious from this table that the C content of soot particles reduced as the blending OME_3 content increased, while the H and O contents as well as the ratio values of H/C and O/C increased. More specifically, the O content of soot particles exhibited an approximate 1.9–8.6 % increase with increasing OME_3 blending. This rise in oxygen content can be attributed to the inherent presence of bound oxygen in the OME_3 fuel component [75,76], which is in line with the preceding results regarding oxygenated functional groups. Correspondingly, the O/C atomic ratios increased with increasing OME_3 content in the fuel blend. Considering that soot particles with higher O/C atomic ratios have higher reactivity [50,56], an increase in blending OME_3 content would enhance soot oxidative reactivity. In addition, the data regarding the H/C atomic ratios further demonstrate that the soot particles with the addition of OME_3 have higher oxidative reactivity. A higher H/C atomic ratio in soot particles indicates a greater amount of H concentration per C atom, which in turn raises the probability of H being abstracted by either O_2 or the radicals present in the combustion process [77]. This process of H abstraction can create radical sites within soot particles [76], thus accelerating the rate of soot oxidation.

3.5. Oxidative reactivity

The results derived from the XPS, FT-IR, and elemental analysis confirmed that the addition of OME_3 led to an increase in oxygenated functional groups, aliphatic C–H groups, H/C and O/C ratios, in conjunction with a reduction in sp^2/sp^3 ratio. Consequently, these alterations in chemical properties would enhance the oxidative reactivity of soot particles [50,56,61,64,68,76]. To validate the aforementioned effect on the oxidative reactivity of soot particles, the E_a derived from TGA was employed to evaluate the oxidative reactivity. The obtained E_a is illustrated in Fig. 8. The values of E_a exhibited a reduction by as much as 15 % following the addition of OME_3. These results revealed that soot particles, which have more oxygenated functional groups and aliphatic C–H groups, greater H/C and O/C ratios, and a lower sp^2/sp^3 ratio, exhibit higher oxidative reactivity with the addition of OME_3. It means that soot particles, which are deposited in DPF from diesel engines with the addition of OME_3, likely have higher oxidative reactivity. This enhanced reactivity in soot particles requires less amount of fuel for their oxidation during the regeneration of the DPF.

It should be noted that the present results were obtained on a McKenna burner with homogeneous laminar flow combustion conditions, which may differ from the results for diesel engines with a distinct combustion process. Although the influential trend of oxygenated fuel addition on the chemical properties of soot particles is consistent by comparing our results with those from diesel engines in the existing literature [32], the obtained results only offer a qualitative guideline for real-world application. Thus, it remains crucial to conduct quantitative assessments under combustion conditions that closely resemble real-world scenarios, such as high-pressure burners, single-cylinder engines, and diesel engines, which, in turn, yield quantitative data for optimising the control strategy of DPF regeneration.

4. Conclusions

To elucidate the impact of OME_3 blending on the chemical properties of soot particles, X-ray photoelectron spectroscopy (XPS), Fourier transform infrared spectroscopy (FT-IR), elemental analyser, and thermogravimetric analysis (TGA) were employed to examine the surface functional groups, hybridized carbon orbital states, elemental compositions, and oxidative reactivity of soot particles generated in an *n*-

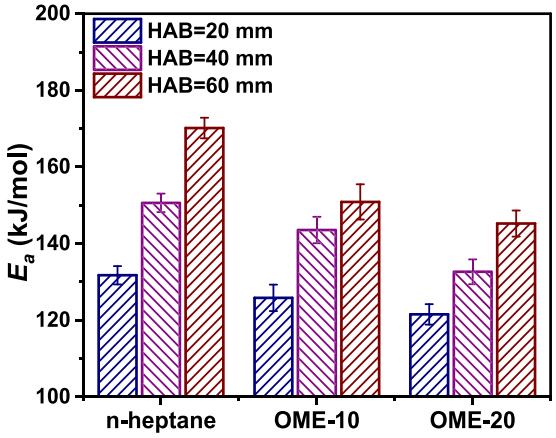

Fig. 8. Activation energy (E_a) for soot particles from *n*-heptane and OME_3 addition at various HABs.

Table 3
Elemental composition (wt.%) for soot samples at various HABs.

	HAB (mm)	C (wt. %)	H (wt. %)	O (wt. %)	H/C atomic ratio	O/C atomic ratio
n-heptane	20	84.35 ± 0.35	2.27 ± 0.07	13.38	0.32	0.13
	40	90.29 ± 0.38	1.31 ± 0.04	8.40	0.17	0.08
	60	93.66 ± 0.23	1.09 ± 0.02	5.25	0.14	0.05
OME-10	20	82.45 ± 0.37	2.32 ± 0.03	15.23	0.33	0.14
	40	85.57 ± 0.31	1.78 ± 0.04	12.65	0.25	0.11
	60	86.89 ± 0.29	1.37 ± 0.04	11.74	0.19	0.10
OME-20	20	81.42 ± 0.28	2.49 ± 0.04	16.09	0.37	0.15
	40	83.47 ± 0.34	1.84 ± 0.03	14.69	0.26	0.13
	60	84.67 ± 0.36	1.48 ± 0.04	13.85	0.21	0.12

heptane/OME_3 inverse diffusion flame. First, the relative contents of C = O, C–O, O = C–O, and aliphatic C − H groups increased with increasing OME_3 doping, whereas aromatic C − H groups reduced. Second, the addition of OME_3 altered the spatial distribution of hybridisation orbitals of carbon atoms, which caused a reduction in the sp^2/sp^3 ratio with increasing OME_3 blending. Third, the addition of OME_3 resulted in higher levels of O and H contents within the soot particles, in line with the surface functional groups above. Finally, activation energy exhibited a reduction by up to 15 % with the addition of OME_3, indicating an increase in the oxidative reactivity of soot particles. These results confirmed that incorporating OME_3 leads to significant modifications in surface functional groups, the spatial distribution of carbon hybridisation orbitals, and elemental composition. These modifications in these chemical properties enhance the oxidative reactivity of soot particles. In addition to these chemical properties, however, the physical properties of soot particles, including morphology, nanostructure, and degree of graphitisation, are also crucial factors affecting oxidative reactivity. In subsequent research, it is necessary to perform further research to gain a more comprehensive understanding of the influence of the addition of OME_3 on soot properties.

CRediT authorship contribution statement

Ye Liu: Writing – original draft, Visualization, Software, Methodology, Investigation, Formal analysis, Conceptualization. **Ran Zhang:** Writing – review & editing, Conceptualization. **Jun Wang:** Writing – review & editing, Validation, Conceptualization. **Yajun Wang:** Writing – review & editing, Validation, Conceptualization. **Gang Lv:** Project administration, Funding acquisition, Conceptualization. **He Yang:** Writing – review & editing, Resources. **Haibo Chen:** Writing – review & editing, Funding acquisition. **Tiezhu Li:** Writing – review & editing, Conceptualization. **Bin Hao:** Writing – review & editing, Methodology. **Junhua Guo:** Conceptualization, Writing – review & editing.

Declaration of competing interest

The authors declare that they have no known competing financial interests or personal relationships that could have appeared to influence the work reported in this paper.

Data availability

Data will be made available on request.

Acknowledgments

This research is supported by the National Energy R&D Center of Petroleum Refining Technology (RIPP, SINOPEC, China), the National Key Research and Development Program of China (No. 2021YFE0112700), the Foreign Expert Project (G2022022004L), and EU-funded projects nPETS (No. 954377).

Appendix A. Supplementary data

Supplementary data to this article can be found online at https://doi.org/10.1016/j.fuel.2024.131422.

References

[1] van DA, Martin RV, Brauer M, Kahn R, Levy R, Verduzco C, et al. Global Estimates of Ambient Fine Particulate Matter Concentrations from Satellite-Based Aerosol Optical Depth: Development and Application. Environ Health Perspect 2010;118:847–55.
[2] Zhang Z-H, Balasubramanian R. Effect of Oxygenated Fuels on Physicochemical and Toxicological Characteristics of Diesel Particulate Emissions. Environ Sci Technol 2014;48:14805–13.
[3] Li D, Wei J, Chen H, Wang C, Wang C. Study on the restructuring of soot particles from diesel engine exhaust gas discharged into a simulated atmospheric environment. Fuel 2023;349:128679.
[4] Liu Y, Chen H, Li Y, Gao J, Dave K, Chen J, et al. Exhaust and non-exhaust emissions from conventional and electric vehicles: A comparison of monetary impact values. J Clean Prod 2022;331:129965.
[5] Sun B, Rigopoulos S. Modelling of soot formation and aggregation in turbulent flows with the LES-PBE-PDF approach and a conservative sectional method. Combust Flame 2022;242:112152.
[6] Wang Y, Chung SH. Soot formation in laminar counterflow flames. Prog Energy Combust Sci 2019;74:152–238.
[7] Cai L, Jacobs S, Langer R, Vom Lehn F, Heufer KA, Pitsch H. Auto-ignition of oxymethylene ethers (OMEn, n = 2–4) as promising synthetic e-fuels from renewable electricity: shock tube experiments and automatic mechanism generation. Fuel 2020;264:116711.
[8] Ferraro F, Russo C, Schmitz R, Hasse C, Sirignano M. Experimental and numerical study on the effect of oxymethylene ether-3 (OME3) on soot particle formation. Fuel 2021;286:119353.
[9] Tan YR, Salamanca M, Pascazio L, Akroyd J, Kraft M. The effect of poly (oxymethylene) dimethyl ethers (PODE3) on soot formation in ethylene/PODE3 laminar coflow diffusion flames. Fuel 2021;283:118769.
[10] He T, Wang Z, You X, Liu H, Wang Y, Li X, et al. A chemical kinetic mechanism for the low- and intermediate-temperature combustion of Polyoxymethylene Dimethyl Ether 3 (PODE3). Fuel 2018;212:223–35.
[11] Verma P, Pickering E, Jafari M, Guo Y, Stevanovic S, Fernando JFS, et al. Influence of fuel-oxygen content on morphology and nanostructure of soot particles. Combust Flame 2019;205:206–19.
[12] García-Oliver JM, Novella R, Micó C, Bin-Khalid U. A numerical investigation of the performance of oxymethylene ethers blended with fossil diesel to reduce soot emissions in compression ignition engines. Fuel 2022;324:124768.
[13] Omari A, Heuser B, Pischinger S. Potential of oxymethylenether-diesel blends for ultra-low emission engines. Fuel 2017;209:232–7.
[14] Pélerin D, Gaukel K, Härtl M, Jacob E, Wachtmeister G. Potentials to simplify the engine system using the alternative diesel fuels oxymethylene ether OME1 and OME3−6 on a heavy-duty engine. Fuel 2020;259:116231.
[15] Parravicini M, Barro C, Boulouchos K. Compensation for the differences in LHV of diesel-OME blends by using injector nozzles with different number of holes: Emissions and combustion. Fuel 2020;259:116166.
[16] Zheng Y, Tang Q, Wang T, Liao Y, Wang J. Synthesis of a Green Fuel Additive Over Cation Resins. Chem Eng Technol 2013;36:1951–6.
[17] Rodríguez-Vallejo DF, Valente A, Guillén-Gosálbez G, Chachuat B. Economic and life-cycle assessment of OME $_{3-5}$ as transport fuel: a comparison of production pathways. Sustainable Energy Fuels 2021;5:2504–16.
[18] Pellegrini L, Marchionna M, Patrini R, Florio S. Emission Performance of Neat and Blended Polyoxymethylene Dimethyl Ethers in an Old Light-Duty Diesel Car. Warrendale, PA: SAE International; 2013.
[19] Pellegrini L, Marchionna M, Patrini R, Beatrice C, Giacomo ND, Guido C. Combustion Behaviour and Emission Performance of Neat and Blended Polyoxymethylene Dimethyl Ethers in a Light-Duty Diesel Engine. Warrendale, PA: SAE International; 2012.
[20] Schmitz R, Russo C, Ferraro F, Apicella B, Hasse C, Sirignano M. Effect of oxymethylene ether-2-3-4 (OME2-4) on soot particle formation and chemical features. Fuel 2022;324:124617.
[21] Schmitz R, Ferraro F, Sirignano M, Hasse C. Numerical and experimental investigations on the particle formation in oxymethylene ethers (OMEn, n = 2–4)/ethylene premixed flames. Fuel 2024;357:129762.
[22] D. Gelner A, Rothe D, Kykal C, Irwin M, Sommer A, Pastoetter C, et al. Particle emissions of a heavy-duty engine fueled with polyoxymethylene dimethyl ethers (OME). Environmental Science: Atmospheres 2022;2:291–304.
[23] Ma M, Rivellini L-H, Kasthuriarachchi N, Zhu Q, Zong Y, Yu W, et al. Effects of polyoxymethylene dimethyl ether (PODEn) blended fuel on diesel engine emission: Insight from soot-particle aerosol mass spectrometry and aethalometer measurements. Atmospheric Environment: X 2023;18:100216.
[24] Arias S, Agudelo JR, Ramos A, Lapuerta M. Emissions from a Euro 6 engine using polyoxymethylene dimethyl ethers: Chemical effects vs mapping strategy. Fuel 2023;335:127017.
[25] Tan YR, Botero ML, Sheng Y, Dreyer JAH, Xu R, Yang W, et al. Sooting characteristics of polyoxymethylene dimethyl ether blends with diesel in a diffusion flame. Fuel 2018;224:499–506.
[26] Song J, Song C, Tao Y, Lv G, Dong S. Diesel soot oxidation during the late combustion phase. Combust Flame 2011;158:446–51.
[27] Jin C, Wei J, Chen B, Li X, Ying D, Gong L, et al. Effect of nanoparticles on diesel engines driven by biodiesel and its blends: A review of 10 years of research. Energ Conver Manage 2023;291:117276.
[28] Wei J, Yin Z, Wang C, Lv G, Zhuang Y, Li X, et al. Impact of aluminium oxide nanoparticles as an additive in diesel-methanol blends on a modern DI diesel engine. Appl Therm Eng 2021;185:116372.
[29] Liu Y, Wu S, Fan C, Wang X, Liu F, Chen H. Variations in surface functional groups, carbon chemical state and graphitization degree during thermal deactivation of diesel soot particles. J Environ Sci 2023;124:678–87.
[30] Liu Y, Fan C, Wang X, Liu F, Chen H. Thermally induced variations in the nanostructure and reactivity of soot particles emitted from a diesel engine. Chemosphere 2022;286:131712.
[31] Guo Y, Ristovski Z, Graham E, Stevanovic S, Verma P, Jafari M, et al. The correlation between diesel soot chemical structure and reactivity. Carbon 2020;161:736–49.

[32] Wei J, Lu W, Zeng Y, Huang H, Pan M, Liu Y. Physicochemical properties and oxidation reactivity of exhaust soot from a modern diesel engine: Effect of oxyfuel type. Combust Flame 2022;238:111940.
[33] Sun C, Martin J, Boehman AL. Impacts of advanced diesel combustion operation and fuel formulation on soot nanostructure and reactivity. Fuel 2020;276:118080.
[34] Lapuerta M, Rodríguez-Fernández J, Sánchez-Valdepeñas J. Soot reactivity analysis and implications on diesel filter regeneration. Prog Energy Combust Sci 2020;78:100833.
[35] Li T, Mitra T, Chu C, Yuan Y, Thomson MJ. Investigation of PAH and soot formation in a dimethyl ether (DME) laminar coflow diffusion flame. Combust Flame 2021;223:437–49.
[36] Liu Y, Song C, Lv G, Fan C, Zhang X, Qiao Y. Relationships between the electrical properties and nanostructure of soot particles in a laminar inverse diffusion flame. Proc Combust Inst 2019;37:1185–92.
[37] Zhao B, Yang Z, Wang J, Johnston MV, Wang H. Analysis of Soot Nanoparticles in a Laminar Premixed Ethylene Flame by Scanning Mobility Particle Sizer. Aerosol Sci Tech 2003;37:611–20.
[38] Liu Y, Song C, Lv G, Wang X, Li N. Virgin and Extracted Soots in Premixed Methane Flames: A Comparison of Surface Functional Groups, Graphitization Degree, and Oxidation Reactivity. Energy Fuels 2017;31:6413–21.
[39] Liu Y, Zhang X, Lyu G, Qiao Y, Zhang W, Song C. Effect of the oxidation-induced fragmentation of primary particles on soot oxidation reactivity. Combust Flame 2022;240:112026.
[40] Mcenally CS, Koylu MO, Pfefferle LD. Soot volume fraction and temperature measurements in laminar nonpremixed flames using thermocouples. Combust. Flame, 109(4), 701-20.
[41] Abdalla AOG, Liu D, Zhang L, Zhao X, Ying Y, Jiang B, et al. Soot formation and evolution in RP-3 kerosene inverse diffusion flames: Effects of flow rates and dimethyl carbonate additions. Fuel 2020;273:117732.
[42] Wang HW, Huang ZH, Zhou LB, Jiang DM, Yang ZL. Technical Note: Investigation on emission characteristics of a compression ignition engine with oxygenated fuels and exhaust gas recirculation. Proceedings of the Institution of Mechanical Engineers, Part D: Journal of Automobile Engineering 2000;214:503–8.
[43] Glaude PA, Pitz WJ, Thomson MJ. Chemical kinetic modeling of dimethyl carbonate in an opposed-flow diffusion flame. Proc Combust Inst 2005;30:1111–8.
[44] Soriano JA, Agudelo JR, López AF, Armas O. Oxidation reactivity and nanostructural characterization of the soot coming from farnesane - A novel diesel fuel derived from sugar cane. Carbon 2017;125:516–29.
[45] Zhang Y, Boehman AL. Oxidation behavior of soot generated from the combustion of methyl 2-butenoate in a co-flow diffusion flame. Combust Flame 2013;160:112–9.
[46] Dames E, Sirjean B, Wang H. Weakly Bound Carbon−Carbon Bonds in Acenaphthene Derivatives and Hexaphenylethane. J Phys Chem A 2010;114:1161–8.
[47] Vander Wal RL, Bryg VM, Hays MD. XPS Analysis of Combustion Aerosols for Chemical Composition, Surface Chemistry, and Carbon Chemical State. Anal Chem 2011;83:1924–30.
[48] Vander Wal RL, Bryg VM, Hays MD. Fingerprinting soot (towards source identification): Physical structure and chemical composition. J Aerosol Sci 2010;41:108–17.
[49] Levi G, Senneca O, Causà M, Salatino P, Lacovig P, Lizzit S. Probing the chemical nature of surface oxides during coal char oxidation by high-resolution XPS. Carbon 2015;90:181–96.
[50] Seong HJ, Boehman AL. Studies of soot oxidative reactivity using a diffusion flame burner. Combust Flame 2012;159:1864–75.
[51] Russo C, Stanzione F, Tregrossi A, Ciajolo A. Infrared spectroscopy of some carbon-based materials relevant in combustion: Qualitative and quantitative analysis of hydrogen. Carbon 2014;74:127–38.
[52] Fan C, Wei J, Huang H, Pan M, Fu Z. Chemical feature of the soot emissions from a diesel engine fueled with methanol-diesel blends. Fuel 2021;297:120739.
[53] Liu Y, Cheng X, Ya Y, Wang B, Zhang P, Zhang K, et al. Impact of PODE3 on soot oxidation reactivity at different stages in n-heptane/toluene diffusion flames. Fuel 2023;331:125672.
[54] Larciprete R, Lacovig P, Gardonio S, Baraldi A, Lizzit S. Atomic Oxygen on Graphite: Chemical Characterization and Thermal Reduction. J Phys Chem C 2012;116:9900–8.
[55] Izquierdo R, García Dos Santos S, Borge R, de la Paz D, Sarigiannis D, Gotti A, et al. Health impact assessment by the implementation of Madrid City air-quality plan in 2020. Environ Res 2020;183:109021.
[56] Song J, Alam M, Boehman AL, Kim U. Examination of the oxidation behavior of biodiesel soot. Combust Flame 2006;146:589–604.
[57] Matti MM. Chemical characterization of particulate emissions from diesel engines: A review. J Aerosol Sci 2007;38:1079–118.
[58] Barinov A, Malcioğlu OB, Fabris S, Sun T, Gregoratti L, Dalmiglio M, et al. Initial Stages of Oxidation on Graphitic Surfaces: Photoemission Study and Density Functional Theory Calculations. J Phys Chem C 2009;113:9009–13.
[59] Szybist JP, Boehman AL, Haworth DC, Koga H. Premixed ignition behavior of alternative diesel fuel-relevant compounds in a motored engine experiment. Combust Flame 2007;149:112–28.
[60] Fanning PE, Vannice MA. A DRIFTS study of the formation of surface groups on carbon by oxidation. Carbon 1993;31:721–30.
[61] Russo C, Tregrossi A, Ciajolo A. Dehydrogenation and growth of soot in premixed flames. Proc Combust Inst 2015;35:1803–9.
[62] Liu Y, Song C, Lv G, Cao X, Wang L, Qiao Y, et al. Surface functional groups and sp3/sp2 hybridization ratios of in-cylinder soot from a diesel engine fueled with n-heptane and n-heptane/toluene. Fuel 2016;179:108–13.
[63] Alfè M, Apicella B, Barbella R, Rouzaud J-N, Tregrossi A, Ciajolo A. Structure–property relationship in nanostructures of young and mature soot in premixed flames. Proc Combust Inst 2009;32:697–704.
[64] Vander Wal RL, Mueller CJ. Initial Investigation of Effects of Fuel Oxygenation on Nanostructure of Soot from a Direct-Injection Diesel Engine. Energy Fuels 2006;20:2364–9.
[65] Marcuccilli F, Gilot P, Stanmore B, Prado G. Experimental and theoretical study of diesel soot reactivity. Symp (Int) Combust 1994;25:619–26.
[66] Mckinnon JT, Meyer E, Howard JB. Infrared analysis of flame-generated PAH samples. Combust Flame 1996;105:161–6.
[67] Blanquart G, Pepiot-Desjardins P, Pitsch H. Chemical mechanism for high temperature combustion of engine relevant fuels with emphasis on soot precursors. Combust Flame 2009;156:588–607.
[68] Santamaría A, Mondragón F, Molina A, Marsh ND, Eddings EG, Sarofim AF. FT-IR and 1H NMR characterization of the products of an ethylene inverse diffusion flame. Combust Flame 2006;146:52–62.
[69] Dobbins RA, Fletcher RA, Chang H-C. The evolution of soot precursor particles in a diffusion flame. Combust Flame 1998;115:285–98.
[70] Dobbins RA, Fletcher RA, Lu W. Laser microprobe analysis of soot precursor particles and carbonaceous soot. Combust Flame 1995;100:301–9.
[71] Vander Wal RL. Soot precursor carbonization: visualization using LIF and LII and comparison using bright and dark field TEM. Combust. Flame, 112(4), 607-16.
[72] Chemical and morphological characterization of soot and soot precursors generated in an inverse diffusion flame with aromatic and aliphatic fuels. Combust Flame 2010;157:33–42.
[73] FT-IR and. 1H NMR characterization of the products of an ethylene inverse diffusion flame. Combust Flame 2006;146:52–62.
[74] Santamaría A, Mondragón F, Quiñónez W, Eddings EG, Sarofim AF. Average structural analysis of the extractable material of young soot gathered in an ethylene inverse diffusion flame. Fuel 2007;86:1908–17.
[75] Gogoi B, Raj A, Alrefaai MM, Stephen S, Anjana T, Pillai V, et al. Effects of 2,5-dimethylfuran addition to diesel on soot nanostructures and reactivity. Fuel 2015;159:766–75.
[76] Luo J, Zhang Y, Wang J, Zhang Q. Effect of acetone–butanol–ethanol addition to diesel on the soot reactivity. Fuel 2018;226:555–63.
[77] Raj A, Yang SY, Cha D, Tayouo R, Chung SH. Structural effects on the oxidation of soot particles by O2: Experimental and theoretical study. Combust Flame 2013;160:1812–26.